Journal of Controlled Release 294 (2019) 226–236

Contents lists available at ScienceDirect

Journal of Controlled Release

journal homepage: www.elsevier.com/locate/jconrel

Enhanced intranasal insulin delivery by formulations and tumor protein-derived protein transduction domain as an absorption enhancer

Nam Ah Kim[a], Ritu Thapa[a], Seong Hoon Jeong[a,*], Hae-duck Bae[b], Jeehye Maeng[b], Kyunglim Lee[b], Kinam Park[c]

[a] College of Pharmacy, Dongguk University-Seoul, Goyang, Gyeonggi 10326, Republic of Korea
[b] College of Pharmacy, Ewha Womans University, Seoul 03760, Republic of Korea
[c] Department of Pharmaceutics and Biomedical Engineering, Purdue University, West Lafayette, IN 47907, USA

ARTICLE INFO

Keywords:
Intranasal absorption
Insulin formulation
Protein transduction domain
Protein aggregation
Carbohydrates

ABSTRACT

One of the key factors for successful development of an intranasal insulin formulation is an absorption enhancer that would deliver insulin efficiently across nasal membranes without causing damage to mucosa or inducing protein aggregation under physiological conditions. In the present study, a protein transduction domain (PTD1) and its L-form with the double substitution A6L and I8A (PTD4), derived from human translationally controlled tumor protein, were used as absorption enhancers. PTD4 exhibited higher compatibility with insulin in terms of biophysical properties analyzed using μDSC, DLS, and CD. In addition, thermodynamic properties indicated stable complex formation but higher propensity of protein aggregation. Arginine hydrochloride (ArgHCl) was used to suppress protein aggregation and carbohydrates (i.e., mannitol, sucrose, and glycerin) were used as osmolytes in the formulation. The relative bioavailability of insulin co-administered intranasally using PTD4, 16 mg/mL glycerin and 100 mM ArgHCl was 58% and that using PTD4, 1 *w/v*% sucrose, and 25 mM ArgHCl was 53% of the bioavailability obtained via the subcutaneous route. These values represented a remarkable increase in bioavailability of intranasal insulin, causing a significant decrease in blood glucose levels within one hour. The pharmacokinetic properties of intranasal absorption were dependent on the concentration of carbohydrates used. These results suggest that the newly designed formulations with PTD represent a useful platform for intranasal delivery of insulin and other biomolecules.

1. Introduction

Conventional Type I diabetes treatment requires frequent subcutaneous injections of insulin which are associated with poor patient compliance, pain, tenderness, local tissue necrosis, infection, and nerve damage at injected sites [1–3]. In the last decade, alternative insulin delivery routes including oral, nasal, pulmonary, and transdermal administration have been extensively explored to overcome the limitations of the conventional treatment [4–6]. However, development of insulin formulations (i.e., tablets, capsules, sprays, or patches) remains challenging due to its poor permeability, instability across different barriers, and requirement of high doses, and low bioavailability [4,7]. Intranasal administration has several advantages over subcutaneous administration including its noninvasive and painless nature and its ability to bypass gastrointestinal (GI) peptidases. Intranasal insulin began attracting attention in Alzheimer's research as well after some human studies reported improved cognition without changes in blood glucose or insulin levels in healthy volunteers [8,9].

However, bioavailability following intranasal administration appears to be < 25% of that following subcutaneous administration [10–14]. Nasulin™, a commercial intranasal insulin product, resulted in 12% absorption relative to its subcutaneous counterpart in healthy volunteers [13]. Moreover, bile salts, surfactants, and fatty acids, which enhanced nasal absorption, caused nasal mucosal damage [10,15,16]. Consequently, new strategies are required to overcome the issues of low bioavailability and mucosal damage.

Recently, protein transduction domains (PTDs), short peptides also known as cell-penetrating peptides (CPPs) derived from the N-terminus of human translationally controlled tumor protein with the sequence of 'MIIYRDLISH', have exhibited the ability to deliver a variety of biopharmaceuticals [17]. The peptides were internalized through lipid raft-dependent endocytosis and partial micropinocytosis, and did not enter lysosome and nucleus [17]. In addition, PTD1, which was developed and selected from 35 different PTD variants, did not exhibit

* Corresponding author at: College of Pharmacy, Dongguk University-Seoul, Goyang, Gyeonggi 10326, Republic of Korea.
E-mail address: shjeong@dongguk.edu (S.H. Jeong).

https://doi.org/10.1016/j.jconrel.2018.12.023
Received 1 August 2018; Received in revised form 26 November 2018; Accepted 13 December 2018
Available online 14 December 2018
0168-3659/

any toxic effects even after seven days of repeated insulin-PTD1 administration in an animal model [18,19]. Moreover, PTD1 was able to enhance nasal absorption of insulin, thereby increasing bioavailability from 1.0% (without PTD1) to 21.3% as compared with subcutaneous administration [19]. However, the solvent used was comprised of only 5 mM sodium phosphate buffer at pH 7.8 with 1:2 M ratio of insulin/PTD1 mixture. Further studies were then needed to optimize the solution as well as PTD sequence to increase insulin biophysical stability and its bioavailability, since insulin penetration across biological membranes into systemic circulation was dependent on its biophysical properties [20]. Insulin penetration is expected to increase if hexameric insulin shifts to dimeric or monomeric one, similar to the observation in subcutaneous injection [20].

Several challenges confront the development of intranasal insulin formulations in terms of biophysical properties because most therapeutic proteins have marginal stability and are susceptible to detrimental effects due to even slight environmental changes, affecting therapeutic activity [21]. Previous studies have addressed conformational changes of various proteins including protein folding/unfolding, aggregation, and fragmentation due to the changes in pH, protein concentration, pharmaceutical excipients, and storage conditions using micro-differential scanning calorimetry (μDSC) [22–24]. Evidently, the stability of therapeutic proteins varied significantly with protein concentration, pH, buffer, and pharmaceutical excipients affecting protein-protein and protein-water interactions [25]. The generation of nitrogen oxide species (NO_x) by arginine and related compounds also increased protein fragmentation at high temperatures although arginine was effective in preventing protein aggregation [22]. The mechanism of protein stabilization due to carbohydrates was related to preferential exclusion of water molecules surrounding proteins, resulting in an exothermic readout in isothermal calorimetry. This led to protein stabilization in solution resulting in increased storage stability and reversible protein folding [25]. The mechanism could have the potential to reverse multimer formation to monomers via rearrangement of water molecules driven by excess carbohydrates. Similarly, formulation strategies using various excipients with their appropriate concentration could prevent protein aggregation or unfolding and preserve therapeutic efficacy. Development strategy in the study was to overcome any instabilities occurring when insulin was formulated with PTDs. Likewise, effects of pH and buffer were also utilized to investigate biophysical stability of insulin/PTD mixture, since its biophysical properties depending on pH were not fully understood.

Moreover, newly developed PTD4, the L-form of PTD1 with the double substitution A6L and I8A to further improve nasal insulin absorption, was adopted to compare its compatibility with insulin against PTD1. After achieving the stable pH range and corresponding basal buffer for the mixture, evaluation of PTD4 for intranasal delivery of insulin with different concentration of arginine hydrochloride and various excipients (i.e., mannitol, sucrose, and glycerin) were performed with respect to its bioavailability. The formulation strategy was assumed to exhibit synergistic effect of protein aggregation suppressors and excess carbohydrates, which could stabilize insulin/PTD mixture biophysically. Osmolality of the formulation can also induce cells to expand or shrink, enhancing intracellular or extracellular transport mechanism and also stabilize proteins by preferential exclusion [25,26]. Bioavailability of intranasal insulin was expected to be enhanced by newly developed PTD4 and formulation strategies.

2. Materials and methods

2.1. Materials and sample preparation

Recombinant human insulin (insulin) consisting of 51 amino acid residues with molecular weight 5807.57 g/mol was purchased from Sigma-Aldrich (St. Louis, MO, USA). All peptides (Table 1; PTD1 and PTD4) were prepared and purchased from Peptron Co. Ltd. (Daejeon, Korea) and supplied by Ewha Womans University. The purity of the peptides assessed using high-performance liquid chromatography was > 95%. The N-terminals of the peptides were acetylated, and the C-terminals of the peptides were protected via amidation.

Table 1
Protein transduction domains and the sequences used.[a]

Peptide	Sequence	Code
TCTP-PTD 13	MIIFRALISHKK	PTD1
TCTP-PTD 13(A6L, I8A)	MIIFRLLASHKK	PTD4

[a] Two TCTP-PTD derived mutant analogs were used, because they exhibited enhanced cell penetrating activity compared to TCTP-PTD wild-type and the other mutants, with low cytotoxicity [18,19].

After insulin was dissolved in 0.01 N HCl (pH 2.0), it was dialyzed for 24 h at 4 °C in a Cellu Sep® H1 cellulose membrane with a MW cut-off of 1000 Da (Membrane Filtration Products, Seguin, TX, USA). 10 mM sodium phosphate buffer and 10 mM sodium citrate buffer with desired pH and selected excipients were used as a medium. Dialyzed insulin was added to the PTD solution, mixed gently, and adjusted to desired concentrations. Sodium phosphate monobasic dihydrate, sodium phosphate dibasic dihydrate, sodium citrate dihydrate, citric acid, D-mannitol, sucrose, glycerin, L-arginine monohydrochloride, L-methionine, and zinc acetate were purchased from Sigma-Aldrich (St. Louis, Mo, USA). Poloxamer 188 (Lutrol F68®) was obtained from BASF (Ludwigshafen, Germany). All the other reagents used in this study met HPLC-analytical grade standards.

2.2. Intranasal administration in animals

Female wistar rats were purchased from Orient Bio Co., Ltd. (Seongnam, Korea). They were housed under controlled humidity, temperature, and a 12 L:12D lighting schedule. Before the experiment, the animals were fasted overnight and those with a body weight of 165–200 g were selected for the intranasal administration study. They were fasted for 24 h before the experiments but allowed to drink water. All animal experiments were approved by Ewha Womans University's Institutional Animal Care and Use Committee.

Along with an intraperitoneal injection of Zoletil and Rompun mixture of 1:1 (1 mL/kg), insulin or insulin/PTD mixture was applied through each nostril and the animals monitored for one hour (including evaluation of blood insulin levels). In a separate group, sodium phenobarbital (60 mg/kg) was administered and the animals monitored for two hours (evaluation of blood glucose levels). Rats were restrained in a supine position during administration and a total of 10 μL of prepared solutions (5 μL/each nostril) was administered at a 1 cm depth via micropipettes. The dose of insulin was fixed at 100 μM and the PTD concentration varied from 100 to 200 μM.

A 0.25 mL blood aliquot was obtained from the jugular vein using 1 mL tuberculin heparinized syringes at 15, 30, and 60 min after dosing to measure insulin concentration in blood plasma. Plasma was separated by centrifugation at 12,000 rpm for 1 min and stored at −80 °C until analysis. The concentration was determined using a human insulin ELISA kit (Mercodia AB, Uppsala, Sweden) and the absorbance at λ_{max} 450 nm was detected using a microplate reader (POWERSCAN HT, DS Pharma Biomedical Co. Ltd., Osaka, Japan). In addition, blood glucose levels were directly measured using an Accu-Chek® glucose meter (Roche Diagnostics, Seoul, Korea) at 30, 60, 90, and 120 min. The baseline blood glucose levels were in the range of 90–125 mg/dL.

2.3. Pharmacokinetic analysis

Bioavailability (BA) of intranasal insulin was evaluated relative to subcutaneous administration (1 IU/kg). Insulin dissolved in PBS was used for subcutaneous administration. The peak plasma concentration

(C_{max}) and time to reach C_{max} at t_{max} were determined from plasma insulin concentration-time curves. The total area under the insulin concentration curve (AUC) was estimated from the sum of successive trapezoids between each data point. The bioavailability of insulin relative to the subcutaneous administration was calculated using the formula below in which BA, 'n' and 's.c.' represent bioavailability, 'nasal' and 'subcutaneous', respectively.

BA (%) = (AUC_n x $Dose_{s.c.}$) / ($AUC_{s.c.}$ x $Dose_n$) x 100% [27].

2.4. Dynamic light scattering (DLS)

Insulin sizes in various liquid formulations were investigated using a Zetasizer Nano ZS90 equipped with MPT-2 Autotitrator (Malvern Instruments, Worcestershire, UK). All the measurements were performed at a temperature of 15 °C. 1 mL of each prepared solution was loaded into a disposable sizing cuvette (Sarstedt, Numbrecht, Germany) for measuring *Z*-average size, hydrodynamic size, and polydispersity index (PDI). In addition, a disposable capillary cell (Malvern Instruments, Worcestershire, UK) was adopted for the measurement of zeta potential. Each measurement was repeated five times continuously with an interval of 10 s. In case of titration, zeta potential was measured from acidic pH 2.0 to basic pH 10.0 using 0.1 N HCl, 0.05 N HCl, and 0.1 M NaOH. The corresponding factors above were derived with the auto-correlation function using the software Zetasizer version 7.12 (Malvern Instruments, Worcestershire, UK).

2.5. Micro-differential scanning calorimetry (μDSC)

μDSC measurements were performed using a VP-DSC Microcalorimeter (Malvern Instruments, Worcestershire, UK) with 0.51471 cm^3 twin cells for the protein sample and reference. Before μDSC measurements, the samples were degassed under vacuum. Dialysis medium were used as a reference to achieve the baseline curve without protein. Thermal analysis of prepared insulin was done at a scan rate of 1 °C/min from 20 °C to 120 °C. The final thermogram was obtained by subtracting the baseline curve from the thermogram measured with insulin. The final thermograms's normalization was performed using the Microcal LLC DSC plug-in for the Origin 7.0 software package provided with the equipment. The final thermograms were evaluated with thermal transitions to calculate transition melting temperature (T_m), calorimetric enthalpy (ΔH_{cal}), and van't Hoff enthalpy (ΔH_{VH}).

2.6. Circular dichroism (CD) spectroscopy

The secondary structure content of the prepared insulin samples was assessed using a Chirascan-plus spectrometer (Applied Photophysics, Surrey, UK). The prepared samples were degassed and diluted to avoid any issues of excessive absorbance values (> 1.2). After calibration to remove noise, buffers were scanned before every sample measurement. A rectangular quartz cuvette with light path length of 0.2 mm (Hellma Analytics, Müllheim, Germany) was used for the scanning of CD spectra at 10 °C. The temperature was regulated using a Peltier type temperature controller TC125 (Quantum Northwest Inc., Spokane, WA, USA). The measurement was performed from 190 nm to 260 nm in the far-UV wavelength region with a resolution of 1 nm and an average of three scan measurements was used. Spectra were processed to obtain specific CD spectra and secondary structure content of insulin using a Pro-Data viewer and CDNN software provided with the equipment.

2.7. Size-exclusion chromatography (SEC)

Various concentrations of insulin and prepared samples were analyzed using an Agilent high performance liquid chromatography system (Agilent HPLC 1260, Santa Clara, CA, USA) with a diode array detector at a wavelength of 280 nm with a TSK-GEL G3000SWXL SEC column (TOSOH Bioscience, King of Prussia, PA, USA). To separate soluble insulin based on size, a mobile phase containing 100 mM sodium phosphate (pH 7.4) and 100 mM sodium chloride were used at a flow rate of 0.8 mL/min. The injection volume was 20 μL. The peak areas for multimers and dimers were combined to calculate the total amount of soluble aggregates. The difference in the total area of insulin peaks (sum of all SEC peaks in each chromatogram) at any point versus those of 0.01 N HCl was considered to represent formation of insoluble aggregates. The percentage of remaining insulin relative to the total peak area with 0.01 N HCl was calculated using the following equation,

$$\%\text{Remaining} = (a_t \div A_0) \times 100.$$

where a_t is the peak area of individual species in any given environment and A_0 is the total peak area of all the species with 0.01 N HCl. Standard deviation of three individual measurements was obtained and plotted as error bars.

3. Results

3.1. Biophysical properties of insulin depending on pH, concentration, and addition of PTDs

3.1.1. Hydrodynamic size of insulin

DLS, a tool to detect protein size distribution, was used to evaluate insulin *Z*-average, size distribution, and PDI. Z-average is the average size of the components including fragments, monomers, and aggregation, and is sensitive to aggregation. PDI is a dimensionless value from 0 to 1 indicating polydispersity of the protein solution. A lower PDI value indicates greater mono-dispersion of particles. Fig. 1 shows insulin size variation from concentrations of 12.5 to 100 μM at pH 2.0 and 7.4, where y-axis in volume percentage and x-axis in nanometer with logarithmic scale. Based on the previous study, hydrodynamic diameters of monomeric, dimeric, and hexameric insulin in solution were 2.7 ± 1.4, 3.8 ± 2.1, and 5.5 ± 1.6 nm, respectively [28]. In comparison, 100 μM insulin in HCl solution was mainly monomeric and monodispersed, distributed in a nano-range from 2.0 to 2.8 nm with the lowest PDI value (Fig. 1a). However, the size distribution of 50 μM insulin increased to 5.4–6.8 nm at pH 7.4, suggesting hexameric insulin (Fig. 1b). *Z*-average also increased to 90.8 nm suggesting protein aggregation or higher multimeric states. The insulin solution was serially diluted to 25 μM to evaluate reversibility of hexamer formation and aggregation. The size distribution of the 25 μM insulin solution decreased to 2.9–3.4 nm, but the Z-average increased to 242.6 nm. The results were consistent with those of earlier investigations demonstrating insulin's instability at alkaline pH and its relatively better stability at acidic environment [29].

In addition, the free energy of insulin unfolding does not decrease at acidic pH 2.0 [30]. As a result, any pre-handling of insulin such as drug loading into polymers is performed at acidic pH to retain the monomeric form and stability and to increase loading efficiency [31–34]. However, all living organisms as well as humans are sensitive to highly acidic solutions and may not tolerate prolonged contact [35]. Subsequent experiments investigated the effect of pH on insulin in terms of solubility and zeta potential, in addition to its compatibility with PTDs.

3.1.2. pH-dependent solubility and zeta potential of insulin and PTDs

Fig. 2a represents the pH-dependent solubility profile of a stock solution of 100 μM insulin in 0.01 N HCl (pH 2.0) dialyzed into buffers of different pH and composition (i.e., citrate buffer at pH 4.4–5.6 and phosphate buffer at pH 6.0–7.6). The solubility of insulin at pH 2.0 and 4.4 was similar, but it gradually decreased at pH 6.0, and the insulin solution turned turbid at pH 4.8 to 5.6 suggesting protein aggregation or hexameric suspension (Fig. 2e). The solution showed the most precipitation at pH 5.2. However, the solubility recovered as the pH increased. The turbidity was assumed to be protein aggregation.

Zeta potential is a factor that results in electrical repulsion with

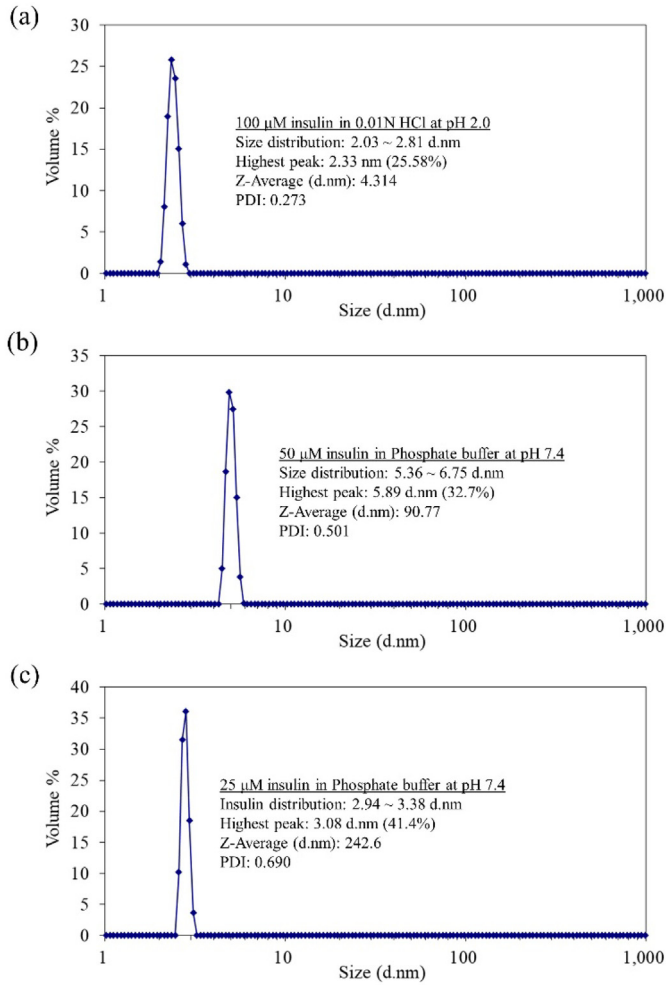

Fig. 1. The hydrodynamic size distribution of (a) 100 μM insulin at pH 2.0, (b) 100 μM insulin at pH 7.4, and (c) 25 μM insulin at pH 7.4. The distribution was represented as a histogram with a size range from 0 to 100 nm on the x-axis.

neighboring particles or surrounding environment [36]. Recent studies have suggested that protein aggregation occurred when the values decreased below ± 10 mV [22,23]. Zeta potential of 10 μM insulin was measured from pH 2.0 to 10.0 via titration (Fig. 2b). Insulin was diluted by 1/10 fold to avoid any problems with viscosity which is inversely proportional to zeta potential [37]. In addition, large particles derived from a concentrated solution are less mobile than those from a dilute sample resulting in a decreased absolute zeta potential. Zeta potential measured from pH 5.0 to 6.0 showed the lowest absolute values and was zero at pH 5.4 suggesting the isoelectric point (p*I*) of folded insulin in solution. On the other hand, the absolute value was greatly increased as pH moved away from the p*I* suggesting an increase in electrical repulsion, which increased its solubility.

Zeta potential of PTD1 and PTD4 without insulin was measured via titration from pH 2.0 to 10.0. Both PTDs exhibited strong positive charges throughout the pH range (Fig. 2c). PTD4 exhibited a relatively higher positive charge than PTD1 at acidic conditions up to a pH of approximately 7.3. In contrast, both PTDs exhibited a decrease in zeta potential as pH continuously increased, because the theoretical p*I* values of the PTDs were approximately at 11.69 calculated by Pepdraw. The net charge of each PTD was expected to be [+ 4] up below pH 6.0 and [+ 3] below pH 10.0 owing to their electrical charge profiles due to positively charged amine groups of arginine, histidine (i.e., [+ 1] at acidic), and two lysine. Therefore, the positively charged PTDs were expected to bind negatively charged insulin, forming a complex. 200 μM PTDs and 100 μM insulin were mixed together at pH 2.0, 4.4, 6.4, and 7.6 to observe their miscibility (Fig. 2f). All solutions were clear except the solution at pH 7.6 which turned cloudy as soon as they were mixed together. This suggested protein aggregation or formation of a hexameric suspension because the solution containing insulin alone was clear despite of high polydispersity. Insulin at pH 7.6 with PTD1 showed precipitation whereas insulin with PTD4 was a suspension-like solution. Nevertheless, the study at pH 7.6 was discontinued to focus more on the effectiveness of PTD as an absorption enhancer for intranasal administration.

Mixing 200 μM PTDs individually with 100 μM insulin at different pH levels resulted in significant changes in zeta potential (a difference of 5 mV was considered significant based on the prior experience). At pH 2.0, the zeta potential of insulin was almost doubled due to the PTD addition, since the positively charged PTDs and insulin were simply added. Likewise, the positive net zeta potential values of insulin and PTD mixtures at selected pH levels were evident from the data shown in Fig. 2b, c, and Table 2. The net values with PTD1 were mostly positive up to pH 6.8 although insulin was negatively charged. The net values were zero at pH 7.0, 7.2, and 7.4. In contrast, the net zeta potential values due to the addition of PTD4 were close to zero or one at pH 4.4. The values strongly indicating protein aggregation because all the net values were less than ± 10 mV as mentioned before. Nevertheless, the above results could also indicate that the net zeta potential value of a solution of insulin and PTDs was dependent on PTD charge, because PTD4 had a higher positive charge than PTD1 (from pH 2.0–7.3) resulting in a net value close to zero. The net values were dependent on charge and concentration of PTDs from 50 to 200 μM (Table 3). As the concentration increased, zeta potential decreased to zero, strongly suggesting complex formation between insulin and PTD.

3.1.3. Intranasal absorption of insulin with PTDs

20 μL of each 100 μM insulin solution with 200 μM PTDs in citrate buffer at pH 4.4 was pipetted into rat nostrils. Plasma insulin concentrations were plotted against time and the plots are illustrated in Fig. 2d. PTDs exhibited the possibility of rapid action with a C_{max} of 15 min. Insulin with PTD4 showed enhanced absorption and increased AUC compared to insulin without PTDs. In contrast, the effect of PTD1 as an absorption enhancer was relatively lower than that of PTD4 at pH 4.4. This might suggest that zeta potential of PTDs is related to insulin absorption efficiency since weaker zeta potential of PTD1 is detected at pH 4.4 (Fig. 2c). Additional zeta potential measurements were performed to observe the net zeta potential value of inulin/PTDs mixture.

Fig. 3 shows zeta potential values of insulin with PTD1 and PTD4. The compatibility of the complexes can be distinguished directly from the graph. Insulin showed two separate zeta potential peaks with PTD1 (Fig. 3a), but a single peak with PTD4. This suggests that PTD4 had a relatively higher interaction with insulin to form a complex, neutralizing the charge of insulin. However, the complex had a high potential of protein aggregation as shown in Fig. 2f. Subsequent experiments addressed the change in conformational stability due to the PTDs.

3.2. Conformational stability of insulin with PTD1 and PTD4

3.2.1. Thermodynamic stability

A typical μDSC thermogram of 100 μM insulin in 0.01 N HCl at pH 2.0 (solid black line) is presented in Fig. 4. The T_m of insulin was 55.6 °C (Fig. 4, Table 4). The result indicates changes in protein folding due to temperature, from monomer to dimer, dimer to oligomer, or monomer to unfolded state. However, DLS results showed that the size distribution at pH 2.0 corresponded to a monomeric solution. Typically, this occurs during thermal transition when van't Hoff enthalpy is greater than calorimetric enthalpy. Thermodynamic parameters listed in Table 4 show the ratio of $\Delta H_{VH}/\Delta H_{cal}$, and the ΔH_{VH} was greater than ΔH_{cal} indicating oligomer formation. Thus, the thermal transition of

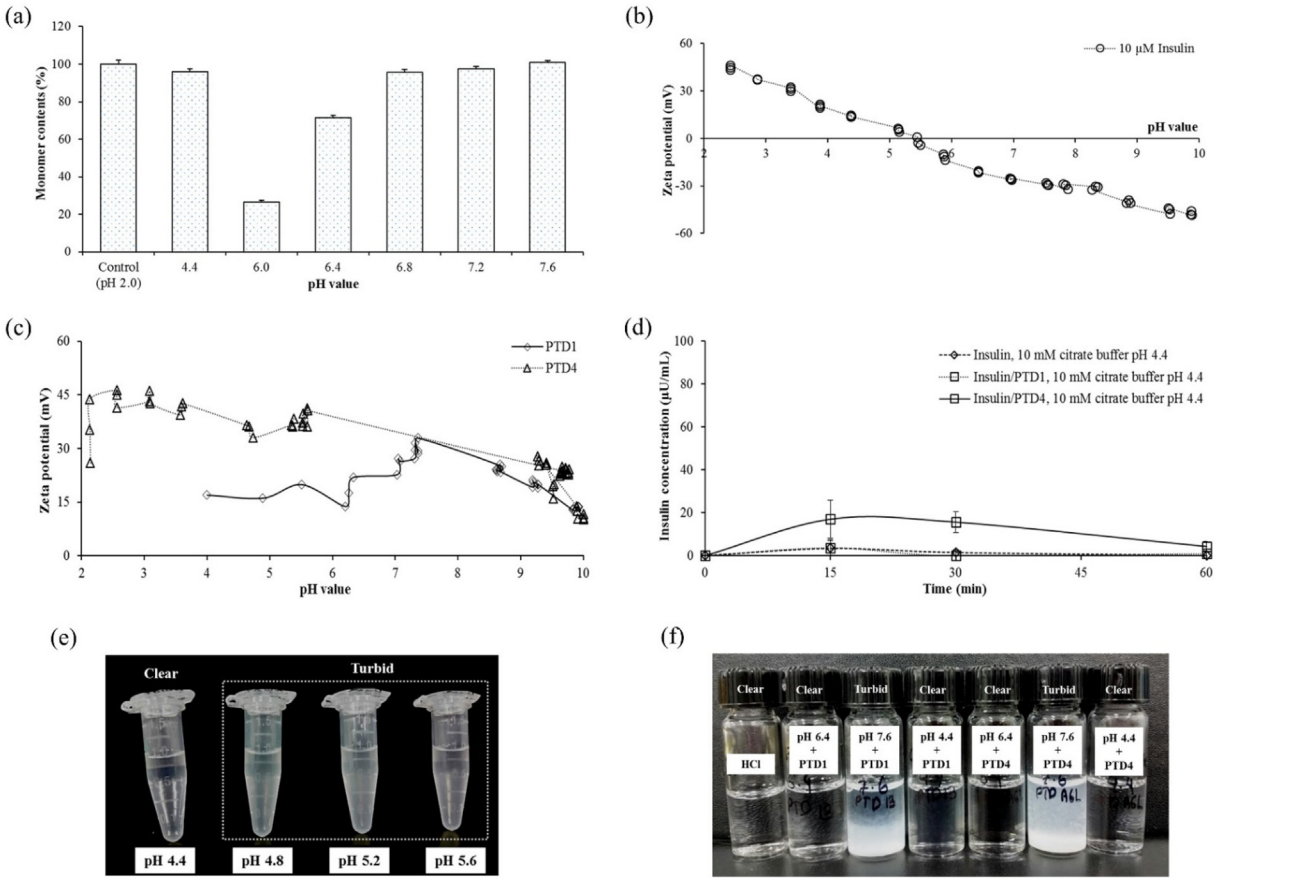

Fig. 2. Plots showing (a) insulin solubility measured using SEC after dialysis into desired pH and buffer, zeta potential of (b) 10 μM insulin and (c) PTDs at a pH range from 2 to 10 adjusted using an autotitrator loaded with 0.1 N HCl, 0.05 N HCl and 0.1 M NaOH. (d) pharmacokinetic profile after intranasal administration of 100 μM insulin in 10 mM sodium citrate buffer at pH 4.4 with PTD1 or PTD4 to rats. Optical observation of insulin (e) at pH 4.4, 4.8, 5.2, and 5.6 and (f) at pH 4.4, 6.4, and 7.6 with PTD1 or PTD4.

Table 2
Zeta potentials measured using DLS at different pH values, with and without 200 μM PTD1 and PTD4.

	Only buffer		+ 200 μM PTD1		+ 200 μM PTD4	
100 μM insulin	ZP (mV)	SD	ZP (mV)	SD	ZP (mV)	SD
pH 2.0	36.23	9.55	77.00	16.47	63.03	17.3
pH 4.4	11.00	0.14	19.60	8.28	8.89	4.78
pH 6.4	−17.00	1.28	18.00	1.66	−0.21	0.22
pH 6.6	−26.33	2.37	21.47	0.38	−2.72	0.56
pH 6.8	−26.17	2.27	15.73	0.32	1.21	0.54
pH 7.0	−29.30	2.46	−1.55	0.28	−1.07	1.03
pH 7.2	−33.70	1.40	3.28	0.62	2.74	0.25
pH 7.4	−31.80	3.05	1.04	0.88	−0.73	0.17

ZP: zeta potential units in millivolts.
SD: standard deviation of five measurements.

Table 3
Zeta potentials measured using DLS in 10 mM phosphate buffer at pH 7.6 with different concentrations of PTD1 and PTD4.

100 μM Insulin	ZP (mV)	SD
pH 7.6 Phosphate buffer	−40.27	1.19
+ 50 μM PTD1	−17.70	1.55
+ 100 μM PTD1	−13.87	0.81
+ 200 μM PTD1	−1.39	0.22
+ 50 μM PTD4	−27.90	0.35
+ 100 μM PTD4	−16.77	1.04
+ 200 μM PTD4	−0.57	0.74

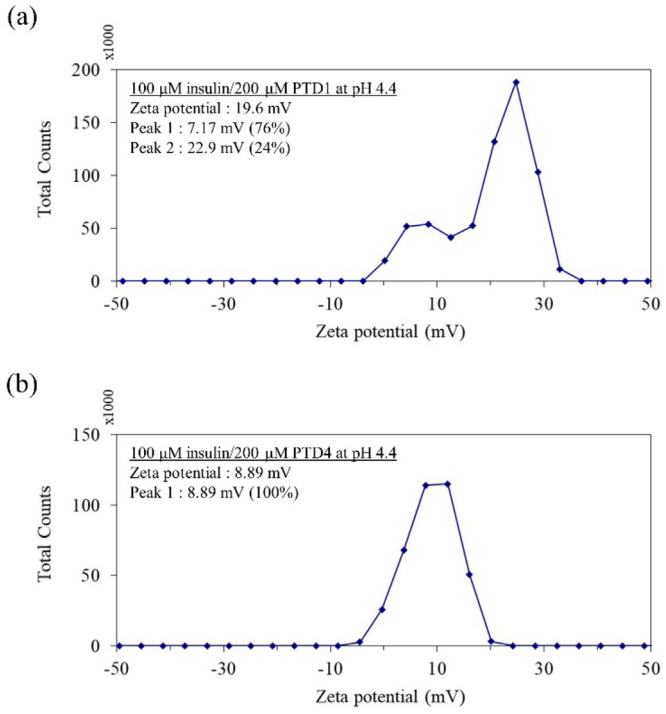

Fig. 3. Zeta potential counts of 100 μM insulin at 10 mM sodium citrate buffer at pH 4.4 with the addition of 200 μM of (a) PTD1 (b) PTD4.

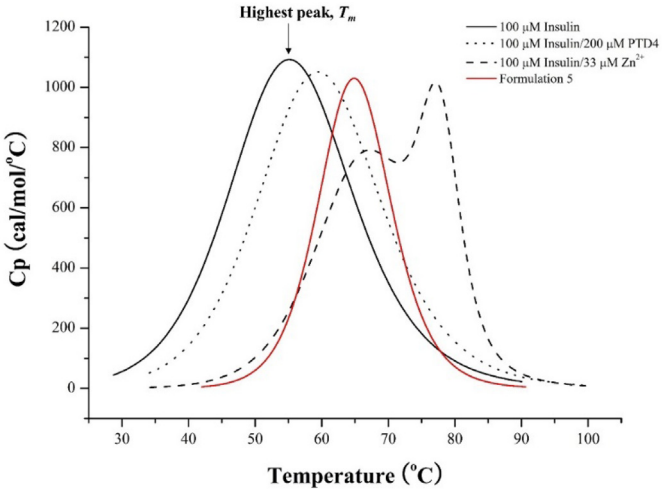

Fig. 4. Typical μDSC thermogram of 100 μM insulin (solid) with 200 μM PTD4 (dotted) and 33 μM zinc ions (dash) and of formulation 5 (red) listed in Table 6. All thermograms were processed and represented using the software Origin 7.0. (For interpretation of the references to colour in this figure legend, the reader is referred to the web version of this article.)

Table 4
Thermodynamic properties of insulin with 200 μM PTD1 and PTD4.

0.01 N HCl (pH 2.0)	T_m (°C)	SD	ΔH_{cal} (cal/mol)	SD	ΔH_{VH} (cal/mol)	SD	$\Delta H_{VH}/\Delta H_{cal}$
100 μM insulin	55.61	0.08	27,000	204	34,730	325	1.29
+ 200 μM PTD1	58.67	0.07	26,460	169	34,570	273	1.31
+ 200 μM PTD4	59.88	0.13	25,820	305	35,850	526	1.39

insulin had a high potential of transition from monomer to dimer or higher oligomer but not a reversible process from a folded to an unfolded state.

A small amount of zinc ions (33 μM) caused a biphasic thermal denaturation pattern of insulin (dashed line), consistent with a previously reported phenomenon [38]. It was concluded that the biphasic denaturation was because of redistribution of zinc ions during heat ramping resulting in two distinct transitions with T_ms values related to monomer/dimer and hexamer, respectively. The first transition (T_m1) was likely to be related to monomer/dimer transition and the second (T_m2; second shoulder) to zinc-hexamer transition because it remains stable at much higher temperatures than the monomer/dimer. The conformational stability of insulin was increased due to addition of zinc ions compared to zinc-free insulin as reflected in the T_m1 value which was almost 67.1 °C, 11.5 °C higher than zinc-free insulin. This may have been because the monomer/dimers could undergo protein aggregation accelerated due to heat resulting in decreased T_m, but the zinc–insulin (hexameric) was relatively more stable against protein aggregation although certain monomer/dimers released from the hexamer caused the biphasic transition.

PTD4 with zinc–insulin (dotted line) also showed increased T_m, higher compared to PTD1 with zinc–insulin but not greater than zinc–insulin alone. In contrast, the PTD4 thermogram did not show any biphasic transitions suggesting that the interaction of PTD and insulin could be higher than that of zinc–insulin, thereby resulting in a difference with the hexameric thermal peak. The propensity of protein aggregation was also increased, reflected in a greater ratio of $\Delta H_{VH}/\Delta H_{cal}$ for PTD–insulin compared to that for zinc-free insulin and PTD1 alone.

3.2.2. Secondary structure stability assessment

The thermodynamic properties evaluated using μDSC were valuable in understanding the conformational stability of insulin and the dominant interaction of PTD–insulin compared to that of zinc–insulin. However, additional analysis such as spectroscopic analyses would be needed to confirm the structural changes [23]. In the present study, CD was used to observe structural changes in insulin, as has been utilized in several studies with external stresses or in formulation studies [39–45]. Protein ellipiticity can be measured as a function of wavelength at a given temperature. Fig. 5, depicting all far-UV CD spectra of insulin in different environments, shows two minima around 210 nm and 225 nm which are commonly observed with predominant α-helical character as reported in several studies [45–49]. All peaks shifted towards decreased intensity with increasing temperature, indicating a loss of α-helical structure. The shift was detected at all elevated temperatures because the onset transition temperature of insulin at pH 2.0 was around 30 °C (Fig. 4). A similar phenomenon (i.e., decreased intensity) was also observed at different insulin concentrations (Fig. 5b), suggesting temperature-dependent loss of α-helical structure approximately 75 μM of insulin. However, reversibility of α-helix loss was confirmed based on CD spectra after cooling the solution to room temperature. In contrast, the intensity after heating and cooling was decreased with two minima at approximately 210 nm and 225 nm (Fig. 5c). The difference in intensity could suggest loss of insulin via protein misfolding or aggregation which might have been accelerated by heat. Simultaneously, absorbance also decreased with a decrease in concentration. The linearity (R^2) of four known concentrations was plotted against absorbance and was 0.998 and 0.993 at 210 nm and 225 nm, respectively, suggesting that the α-helical contents decreased in a concentration-dependent

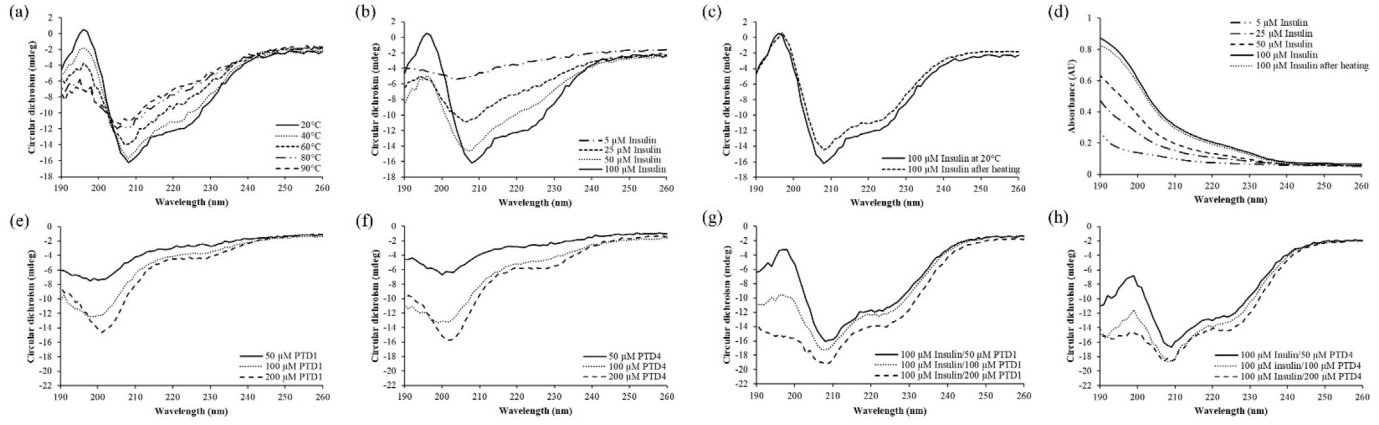

Fig. 5. CD spectra of (a) 100 μM insulin with heat ramping from 20 to 90 °C, (b) insulin concentrations from 5 to 100 μM, (c) 100 μM insulin before and after heat ramping and cooling to RT, (e) PTD1 and (f) PTD4 at 50, 100, 200 μM, and insulin mixture with 50, 100, 200 μM of (g) PTD1 or (h) PTD4. (d) Absorbance measured at the same time with different concentrations of insulin, and before and after heat ramping and cooling to RT.

Table 5
Secondary structure content of insulin at different concentrations of PTD1 and PTD4.

Secondary Structure (%)	α-helix	Anti-parallel β-sheet	Parallel β-sheet	β-turn	Random coil
PTD1					
50 μM	31.70	9.10	9.10	17.20	32.90
100 μM	27.14	10.02	10.02	17.41	35.41
200 μM	27.57	9.87	9.87	17.30	35.29
PTD4					
50 μM	31.43	9.24	9.14	17.37	32.93
100 μM	26.18	10.14	10.24	17.39	35.94
200 μM	23.82	10.59	10.87	17.30	37.62

manner and decreased with temperature indicating a propensity towards insulin instability.

CD spectra of PTD1 and PTD4 at different concentrations exhibited a fixed minima peak at approximately 203 nm (Fig. 5e and f). The spectral features are commonly seen with a predominant character of random coil structure as previously reported [50–52]. Fig. 5g and h show CD spectra of 100 μM insulin with PTDs at different concentrations. The intensity of negative peaks at 210 nm and 225 nm appeared to increase with PTD concentration but the positive peak at approximately 197 nm decreased with increase in PTD concentration, which was influenced by random coil spectra at 203 nm. Changes in secondary structure content were evaluated using a CDNN method and the data are shown in Table 5 (i.e., α-helix, anti-parallel β-sheet, parallel β-sheet, β-turn, and random coil). A wavelength range from 190 nm to 260 nm was used to determine secondary structure content because light at lower wavelengths affects the detected signal more due to increased light scattering [53]. PTDs with insulin showed a decrease in α-helix and increase in random coil content. On the other hand, there was no significant change in β-sheets or β-turns; a difference in content < 1% was not considered meaningful based on our experience.

3.3. In vivo bioavailability of various formulations

3.3.1. Effects of formulation factors: pH and excipients

Nasal administration in rats was performed using insulin solutions at pH levels from 6.4 to 7.4 with PTD4 (Fig. 6a). The highest insulin absorption was observed at pH levels from 6.5 to 7.0. However, the absorption decreased above pH 7.2 and was the lowest at pH 7.6.

Table 6
Summary of 11 formulations of intranasal insulin and the corresponding relative bioavailability (BA) with transition melting temperatures.

Formulation	Carbohydrate	ArgHCl (mM)	BA (%)	T_m (°C)	SD
1	250 mM Mannitol	0	2.4	63.5	0.0
2	n/a	150	35	62.3	0.1
3	150 mM Mannitol	100	46	63.3	0.1
4	1 w/v% Sucrose	25	53	64.0	0.4
5	1 w/v% Sucrose	100	48	64.9	0.1
6	3 w/v% Sucrose	100	50	63.0	0.2
7	16 mg/mL Glycerin	0	42	66.1	0.1
8	16 mg/mL Glycerin +1 w/v% Sucrose	0	23	65.1	0.1
9	16 mg/mL Glycerin	100	58	63.3	0.1
10	30 mg/mL Glycerin	100	21	61.1	0.1
11	30 mg/mL Glycerin +1 w/v% Sucrose	100	13	56.3	0.2

Consequently, formulation studies were continued with the same default formulation; 10 mM phosphate buffer at pH 7.0, 200 μM PTD4 as an absorption enhancer, 0.5 mg/mL poloxamer 188 as a surfactant, 1 mM methionine as an antioxidant, and 33 μM zinc to induce hexamer of free insulin for better physical stability.

250 mM mannitol, which is known to be a protein stabilizer, either decreased or did not affect insulin absorption but 150 mM arginine hydrochloride (ArgHCl) increased insulin absorption and increased BA to 35% (Table 6). The absorption was rapid and insulin concentration in blood was the highest at 15 min (t_{max}). However, BA also increased to 46% when 100 mM ArgHCl and 150 mM mannitol were both added (Fig. 6b). In addition, the mixture showed extended insulin absorption thereby shifting t_{max} towards 30 min. In summary, ArgHCl was effective for insulin with PTD4 mixture in increasing insulin absorption. The effect was assumed to be related to colloidal protein stability and suppression of protein aggregation, but not protein refolding or conformational stability [22,54]. On the other hand, a high level of mannitol could not enhance absorption although carbohydrates are known to be protein stabilizers. It is commonly thought that concentrated carbohydrates or sugars act as osmolytes, surrounding the hydrodynamic surface of proteins and affect protein folding. This is known as preferential exclusion [25,55]. Such preferential exclusion appeared to be ineffective on insulin absorption at 250 mM mannitol alone. However, the mixture of 150 mM mannitol and 100 mM ArgHCl showed a

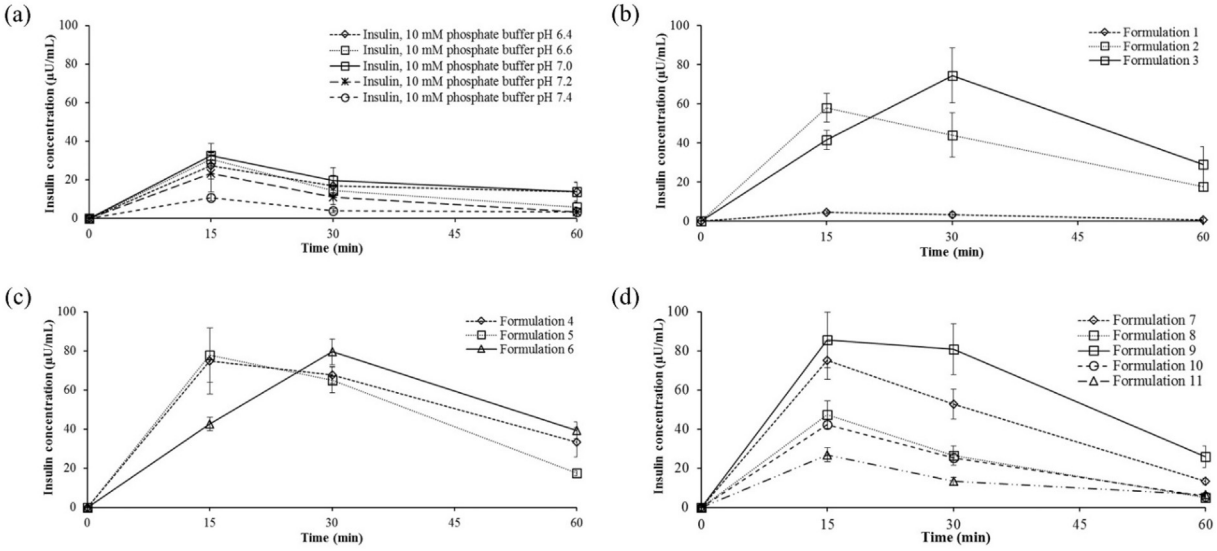

Fig. 6. Pharmacokinetic profiles of insulin in blood plasma against time for (a) 100 μM insulin with 200 μM PTD4 at pH 6.4 to 7.4, (b) mannitol-based Formulations 1 to 3, (c) sucrose-based Formulations 4 to 6, and (d) glycerin-based Formulations 7 to 11.

synergistic effect. Subsequent experiments were carried out with different types of carbohydrates, sucrose and glycerin.

Mixtures of 1 *w/v*% sucrose with 25 mM or 100 mM ArgHCl showed similar absorption kinetics with identical t_{max} values of 15 min (Fig. 6b). BA of Formulations 4, 5, and 6 with sucrose were relatively higher than that of mannitol formulations (Table 6). On the other hand, Formulation 6 also prolonged t_{max} to 30 min and increased BA up to 50% due to increased sucrose concentration from 1 w/v% to 3 w/v%. Sucrose and mannitol showed a potential to control insulin absorption into nasal capillaries because absorption at 15 min was reduced but the constant rate still caused a change in t_{max}. In contrast, certain glycerin formulations showed different absorption profiles and pharmacokinetic properties.

BA of insulin at 16 mg/mL glycerin was increased to 42%, which further increased to 58% when mixed with 100 mg/mL ArgHCl, resulting in the highest BA in the present study. Nevertheless, the t_{max} was not changed although glycerin concentration was increased to 30 mg/mL. 16 mg/mL glycerin with 100 mM ArgHCl resulted in extended absorption until 30 min, contributing to the maximal BA. Consequently, mannitol, sucrose, and glycerin showed a synergistic effect with ArgHCl in insulin absorption in the presence of PTD4, but glycerin did not show any synergistic effect with sucrose.

3.3.2. Blood glucose levels

Fig. 7 shows the blood glucose level measured within two hours after administration of 100 μM insulin and 200 μM PTD4 at pH 6.5 and 7.0. The formulations were significantly more effective than insulin alone. Insulin alone did not result in a decrease in blood glucose level, but the insulin formulations significantly decreased the level, being effective for one hour (Fig. 7a). The glucose level shifted to the recovery phase after an hour administration. In addition, the decrease in glucose level was relatively higher at pH 6.5 than at pH 7.0. This suggests a correlation between nasal pH and insulin absorption. On the other hand, the blood glucose level decreased in a PTD4 concentration-dependent manner. The effect was lesser when the PTD4 concentration was decreased from 200 μM to 100 μM. PTD4 was found to be effective in insulin absorption and in the effectiveness of the formulation.

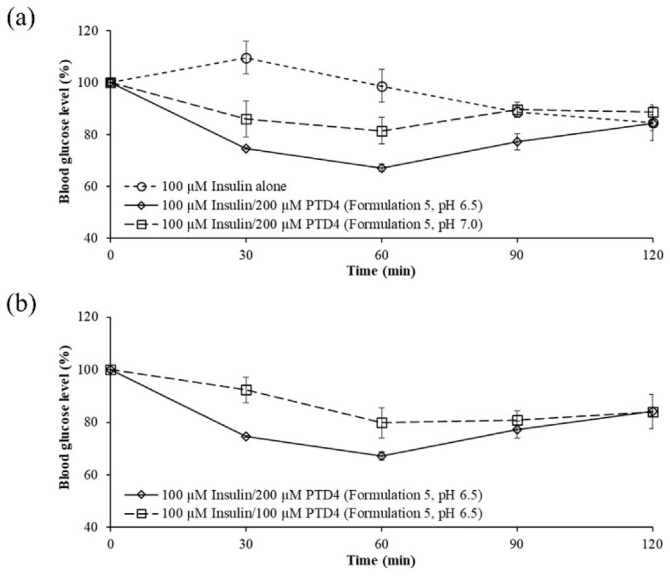

Fig. 7. Pharmacokinetic profiles of glucose level in blood against time for (a) 100 μM insulin (dotted) with 200 μM PTD4 at pH 7.0 (dash) and at pH 6.5 (solid), and (b) 100 μM insulin with 100 μM (dash) and 200 μM (solid) PTD4 at pH 6.5.

4. Discussion

Despite the available strategies for the management of Type 1 diabetes, new approaches involving the formulation of various pharmaceutical forms of insulin into sprays for inhalation via the nose have been in development. However, the biophysical stability of insulin in route of transport requires further optimization including long-term storage stability and also increasing its bioavailability. Present studies suggest useful formulation candidates for such concerns at clinical trials for diabetes for newer approaches in treatment of conventional diabetes by eliminating needle pains and increasing patient compliance and safety [56–59]. For treatment of diabetes, it is critically important to deliver the right amount of insulin at the right time. Currently, nasal insulin delivery may not be able to achieve the right dose at the right time delivery, but significant bioavailability of nasal insulin delivery provides the first step towards achieving such a goal.

The major obstacles to protein absorption include challenges in transmembrane transport because of the large size of proteins (i.e., > 1 kDa), rapid mucociliary clearance, and enzymatic degradation [60], resulting in low protein bioavailability in the absence of absorption enhancers [61,62]. In the present study, newly developed PTDs were evaluated as absorption enhancers based on a study showing their non-toxic nature and potential utility in enhancing nasal insulin delivery [59]. Of the two PTDs evaluated (Table 1), PTD4, an L-form of PTD1 containing the double substitution A6L and I8A was selected for further pharmacokinetic studies because it showed better compatibility with insulin in terms of biophysical properties. Both PTD1 and PTD4 showed positive zeta potential throughout the selected pH range and PTD4 was relatively better than PTD1 in neutralizing negatively charged insulin from pH 4.4 to 7.4 (i.e., a net value close to zero) (Table 2). In addition, the mixture of charged insulin with PTD4 was distributed homogeneously whereas the mixture of insulin and PTD1 showed two different charge distributions (Fig. 3). This suggests that PTD4 has a greater interaction with insulin, thereby forming a complex more effectively. However, a stronger interaction can also result in instability in protein folding. μDSC and CD were used to evaluate such effects. First, T_m measured using μDSC revealed a change in conformational stability of insulin, increasing from 55.61 °C to 59.88 °C due to the addition of PTD4. PTD1 also increased T_m but not more than PTD4 did. On the other hand, the ratio of $\Delta H_{VH}/\Delta H_{cal}$ showed a contrasting trend. A ratio greater than one suggests that proteins can form dimers, tetramer, or higher oligomers during the reaction [63]. In this case, PTD4 had a higher value than PTD1 or insulin alone suggesting a higher propensity towards protein aggregation as shown in Fig. 2f. This suggested that the insulin-PTD complex needed aggregation suppressors to increase colloidal stability in an aqueous state. Second, CD was used to examine the propensity of biophysical changes in terms of secondary structural stability. As the temperature increased, the α-helix dominant CD spectrum of insulin was shifted towards a pattern similar to the CD spectra of diluted samples (Fig. 5a and b), showing a decreased signal but reversibility upon heating. Random coil-dominant PTDs resulted in insulin CD spectra shifting in the opposite direction (i.e. against decrease in depth) as that of protein unfolding due to heat (Fig. 5g and h). In addition, the depth of random coil spectra increased at approximately 200 nm. As a result, secondary structure content calculated using CDNN showed an increase in random coil content. The PTDs did not induce protein unfolding in terms of CD spectra of the complexes but increased random coil content with 200 μM PTD4 resulting in the highest value of all. This difference suggests an association with enhanced conformational stability, which was already indicated by the μDSC results. However, CD analysis with the formulations were not continued because the excipients used produced spectral noises in the far-UV region [64]. Along with PTD4 as an absorption enhancer, various excipients were used to evaluate bioavailability of insulin in vivo.

The three main factors considered in developing intranasal

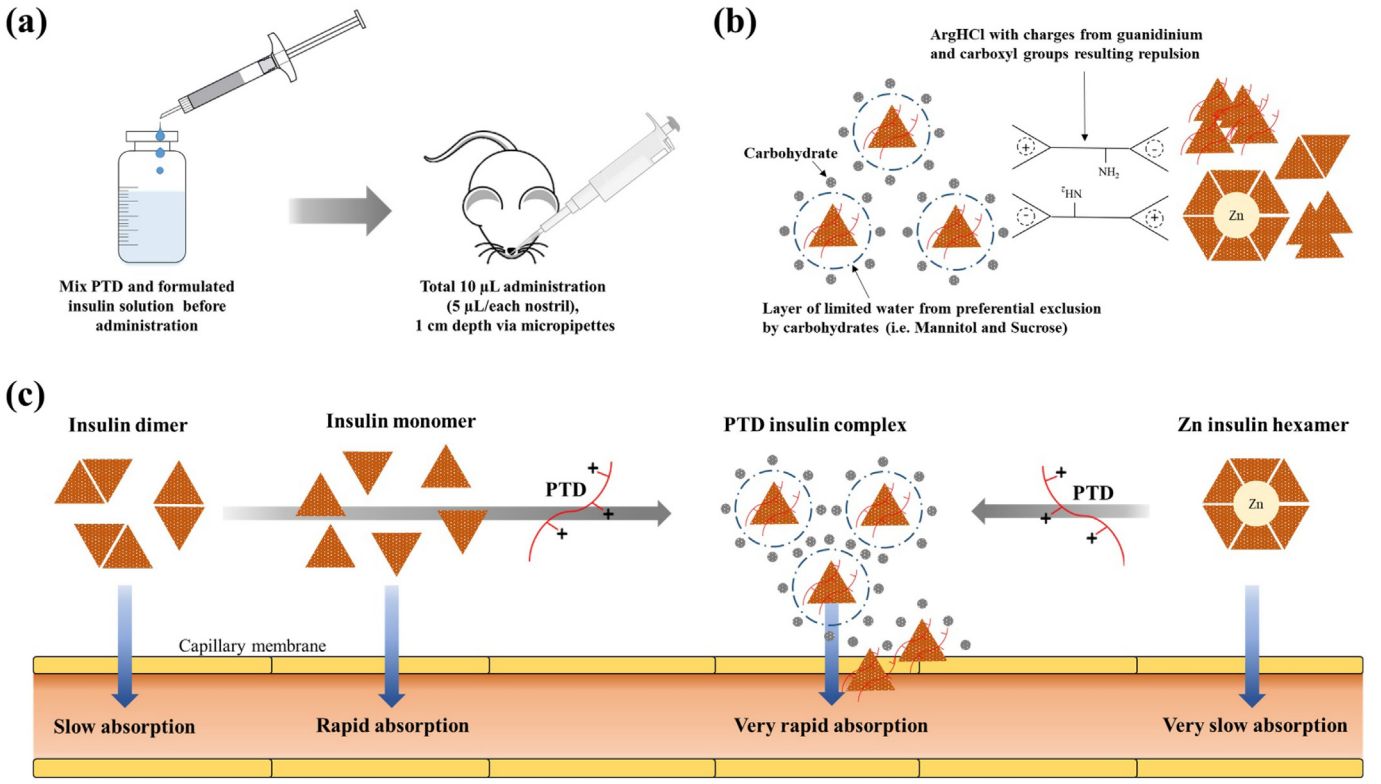

Fig. 8. Schematic illustration of (a) intranasal insulin administration with PTD, (b) combination effect of ArgHCl [24] and carbohydrates [27] on protein aggregation and osmotic pressure, and (c) insulin association states with different absorption rates.

formulations in the present study were suppression of protein aggregation, rapid absorption within 20 min, and pH control to avoid nasal irritation and infection. Insoluble protein aggregation in a pharmaceutical protein solution is unacceptable and represents quality failure. Liquid and powdered intra nasal formulations are typically cleared in 15 to 20 min via rapid mucociliary clearance in the absence of a mucoadhesive [65]. Lastly, it is reported that the pH of intranasal formulations must be adjusted to be between 4.5 and 6.5 [66,67]. The pH range from 3 to 10 does not result in morphological changes in the mucosa but affects frequency of ciliary movement, and pH outside the range produces irreversible damage to mucosa [66,67]. Likewise, certain formulations at low pH caused rats to sneeze in the present study (data not shown). Considering the above three factors were considered carefully; ArgHCl selected as a protein aggregation suppressor, carbohydrates routinely used in biopharmaceutics as protein stabilizers and osmolytes (i.e., mannitol, sucrose, and glycerin), and 10 mM phosphate buffer at pH 6.5 and 7.0 as the buffer solution. Zinc ions, surfactant, and antioxidants were included in all formulations to reduce environmental effects due to storage conditions, interactions with containers, or interactions with air and light, respectively. In summary, formulations with ArgHCl showed a significant increase in bioavailability from 2.4% (Formulation 1) to 58% with 100 mM ArgHCl (Formulation 9) and to 53% with 25 mM ArgHCl (Formulation 4). A high concentration of carbohydrates, 3 *w/v*% sucrose and 150 mM mannitol shifted the t_{max} from 15 min to 30 min. This suggests controlled release of insulin from the formulated solution to the blood circulation, inferred based on the preferential exclusion of water molecules surrounding proteins due to carbohydrates [25], thereby inducing a constant osmotic driving force across membranes with PTD4. Alternatively, increase in viscosity may be partially mucoadhesive. However, 16 mg/mL glycerin which is denser than water did not change the t_{max} but resulted in sustained release from 15 min to 30 min producing the highest BA observed in the present study. Glycerin also resulted in 42% BA without ArgHCl indicating its effect as a protein aggregation suppressor and a protein stabilizer, because of which it is widely used as a tonicity agent in commercial insulin products including Lantus®, Novolog®, Humulin®, and Levemir® [68]. In addition, the formulation resulted in the highest T_m, evidencing an insulin stabilizing effect (Table 6). Nevertheless, a synergistic effect with sucrose and glycerin was not observed, and neither was a beneficial effect of increasing glycerin concentration. Both caused a decrease in BA and T_m. Subsequent experiments were conducted with Formulation 5 to evaluate its activity and complex formation since it had relatively higher conformational stability of insulin (T_m value) that resulted in higher storage stability, maintaining above 90% of insulin at accelerated storage condition. The results showed a decrease in blood glucose levels with a further decrease when the pH was adjusted to 6.5 from 7.5, suggesting that the absorption also depends on the physiological status of the nasal cavity (Fig. 7a). Lastly, the blood glucose level also decreased depending on the amount of PTD4 in the formulation (Fig. 7b), confirming its ability as an absorption enhancer and the effectiveness of the formulation, releasing insulin in a rapid manner within 60 min via nasal administration. Throughout the study, the effect of ArgHCl and carbohydrates well as PTD were established and its mechanism is proposed in Fig. 8. Further studies on the complex formation and dissociation after nasal absorption are necessary for timely delivery of the right amount of insulin for diabetic patients. For other applications where the range of insulin amounts can have the same function, the current approach can be developed into a clinically useful formulation.

5. Conclusion

In conclusion, different absorption profiles were evaluated using carbohydrates and arginine to control nasal protein delivery. Further, it was demonstrated that PTD4 (MIIFRLLASHKK) effectively improved nasal absorption of insulin and enhanced the relative bioavailability of insulin by suppressing protein aggregation. Additional studies are clearly necessary to evaluate long-term storage stability as well as

mechanism of absorption, but our findings suggest that the new formulation candidates described can be optimized for effective nasal delivery of insulin and other therapeutics.

Acknowledgement

This work was supported by the National Research Foundation of Korea (NRF) grant funded by the Korea government (MSIT) (NRF-2018R1A5A2023127) and the Basic Science Research Program through the National Research Foundation of Korea (NRF) funded by the Ministry of Education (NRF-2018R1D1A1B07045154).

References

[1] T. Richardson, D. Kerr, Skin-related complications of insulin therapy: epidemiology and emerging management strategies, Am. J. Clin. Dermatol. 4 (2003) 661–667.
[2] K. Buzasi, Z. Sapi, G. Jermendy, Acanthosis nigricans as a local cutaneous side effect of repeated human insulin injections, Diabetes Res. Clin. Pr. 94 (2011) e34–e36.
[3] E. Chantelau, M. Spraul, I. Muhlhauser, R. Gause, M. Berger, Long-term safety, efficacy and side-effects of continuous subcutaneous insulin infusion treatment for type 1 (insulin-dependent) diabetes mellitus: a one Centre experience, Diabetologia 32 (1989) 421–426.
[4] R. Mo, T. Jiang, J. Di, W. Tai, Z. Gu, Emerging micro- and nanotechnology based synthetic approaches for insulin delivery, Chem. Soc. Rev. 43 (2014) 3595–3629.
[5] D.R. Owens, New horizons–alternative routes for insulin therapy, Nat. Rev. Drug Discov. 1 (2002) 529–540.
[6] R.B. Shah, M. Patel, D.M. Maahs, V.N. Shah, Insulin delivery methods: past, present and future, Int. J. Pharm. Investig. 6 (2016) 1–9.
[7] V.B. Lang, P. Langguth, C. Ottiger, H. Wunderli-Allenspach, D. Rognan, B. Rothen-Rutishauser, J.C. Perriard, S. Lang, J. Biber, H.P. Merkle, Structure-permeation relations of met-enkephalin peptide analogues on absorption and secretion mechanisms in Caco-2 monolayers, J. Pharm. Sci. 86 (1997) 846–853.
[8] J. Born, T. Lange, W. Kern, G.P. McGregor, U. Bickel, H.L. Fehm, Sniffing neuropeptides: a transnasal approach to the human brain, Nat. Neurosci. 5 (2002) 514.
[9] C. Benedict, M. Hallschmid, A. Hatke, B. Schultes, H.L. Fehm, J. Born, W. Kern, Intranasal insulin improves memory in humans, Psychoneuroendocrinology 29 (2004) 1326–1334.
[10] E. Marttin, J.C. Verhoef, S.G. Romeijn, F.W. Merkus, Effects of absorption enhancers on rat nasal epithelium in vivo: release of marker compounds in the nasal cavity, Pharm. Res. 12 (1995) 1151–1157.
[11] L. Illum, Nasal drug delivery: new developments and strategies, Drug Discov. Today 7 (2002) 1184–1189.
[12] A.C. Leary, R.M. Stote, H.J. Breedt, J. O'Brien, B. Buckley, Pharmacokinetics and pharmacodynamics of intranasal insulin administered to healthy subjects in escalating doses, Diabetes Technol. Ther. 7 (2005) 124–130.
[13] A.C. Leary, M. Dowling, K. Cussen, J. O'Brien, R.M. Stote, Pharmacokinetics and pharmacodynamics of intranasal insulin spray (Nasulin) administered to healthy male volunteers: infuence of the nasal cycle, J. Diabetes Sci. Technol. 2 (2008) 1054–1060.
[14] X. Duan, S. Mao, New strategies to improve the intranasal absorption of insulin, Drug Discov. Today 15 (2010) 416–427.
[15] S.G. Chandler, N.W. Thomas, L. Illum, Nasal absorption in the rat. III. Effect of lysophospholipids on insulin absorption and nasal histology, Pharm. Res. 11 (1994) 1623–1630.
[16] S.S. Davis, L. Illum, Absorption enhancers for nasal drug delivery, Clin. Pharmacokinet. 42 (2003) 1107–1128.
[17] M. Kim, M. Kim, H.Y. Kim, S. Kim, J. Jung, J. Maeng, J. Chang, K. Lee, A protein transduction domain located at the NH2-terminus of human translationally controlled tumor protein for delivery of active molecules to cells, Biomaterials 32 (2011) 222–230.
[18] M. Kim, J. Maeng, J. Jung, H.Y. Kim, H.J. Kim, Y. Kwon, K. Lee, Design and evaluation of variants of the protein transduction domain originated from translationally controlled tumor protein, Eur. J. Pharm. Sci. 43 (2011) 25–31.
[19] H.D. Bae, K. Lee, On employing a translationally controlled tumor protein-derived protein transduction domain analog for transmucosal delivery of drugs, J. Control. Release 170 (2013) 358–364.
[20] S. Khafagy El, N. Kamei, E.J. Nielsen, R. Nishio, M. Takeda-Morishita, One-month subchronic toxicity study of cell-penetrating peptides for insulin nasal delivery in rats, Eur. J. Pharm. Biopharm. 85 (2013) 736–743.
[21] J. Brange, D.R. Owens, S. Kang, A. Vølund, Monomeric insulins and their experimental and clinical implications, Diabetes Care 13 (1990) 923–954.
[22] C.N. Pace, S. Trevino, E. Prabhakaran, J.M. Scholtz, Protein structure, stability and solubility in water and other solvents, Philos. T. Roy. Soc. B. 359 (2004) 1225–1234.
[23] N.A. Kim, S. Hada, R. Thapa, S.H. Jeong, Arginine as a protein stabilizer and destabilizer in liquid formulations, Int. J. Pharm. 513 (2016) 26–37.
[24] N.A. Kim, D.G. Lim, J.Y. Lim, K.H. Kim, S.H. Jeong, Comprehensive evaluation of etanercept stability in various concentrations with biophysical assessment, Int. J. Pharm. 460 (2014) 108–118.
[25] N.A. Kim, K. Song, D.G. Lim, S. Hada, Y.K. Shin, S. Shin, S.H. Jeong, Basal buffer systems for a newly glycosylated recombinant human interferon-beta with biophysical stability and DoE approaches, Eur. J. Pharm. Sci. 78 (2015) 177–189.
[26] N.A. Kim, R. Thapa, S.H. Jeong, Preferential exclusion mechanism by carbohydrates on protein stabilization using thermodynamic evaluation, Int. J. Biol. Macromol. 109 (2017) 311–322.
[27] S.V. Dhuria, L.R. Hanson, W.H. Frey 2nd, Intranasal delivery to the central nervous system: mechanisms and experimental considerations, J. Pharm. Sci. 99 (2010) 1654–1673.
[28] A. Oliva, J. Fariña, M.A. Llabrés, Development of two high-performance liquid chromatographic methods for the analysis and characterization of insulin and its degradation products in pharmaceutical preparations, J. Chromatogr. B 749 (2000) 25–34.
[29] J.R. Murlin, H.D. Clough, C. Gibbs, A.M. Stokes, Aqueous extracts of pancreas I. Influence on the carbohydrate metabolism of depancreatized animals, J. Biol. Chem. 56 (1923) 253–296.
[30] C. Bryant, D.B. Spencer, A. Miller, D.L. Bakaysa, K.S. McCune, S.R. Maple, A.H. Pekar, D.N. Brems, Acid stabilization of insulin, Biochemistry 32 (1993) 8075–8082.
[31] C. Ramkissoon-Ganorkar, F. Liu, M. Baudyš, S.W. Kim, Modulating insulin-release profile from pH/thermosensitive polymeric beads through polymer molecular weight, J. Control. Release 59 (1999) 287–298.
[32] Z. He, J.L. Santos, H. Tian, H. Huang, Y. Hu, L. Liu, K.W. Leong, Y. Chen, H.-Q. Mao, Scalable fabrication of size-controlled chitosan nanoparticles for oral delivery of insulin, Biomaterials 130 (2017) 28–41.
[33] J. Sheng, H. He, L. Han, J. Qin, S. Chen, G. Ru, R. Li, P. Yang, J. Wang, V.C. Yang, Enhancing insulin oral absorption by using mucoadhesive nanoparticles loaded with LMWP-linked insulin conjugates, J. Control. Release 233 (2016) 181–190.
[34] J.L. Whittingham, D.J. Scott, K. Chance, A. Wilson, J. Finch, J. Brange, G.G. Dodson, Insulin at pH 2: structural analysis of the conditions promoting insulin fibre formation, J. Mol. Biol. 318 (2002) 479–490.
[35] J.E. Gern, A.G. Mosser, Acidic buffered nasal spray, Google Patents, 2001 US6187332B1.
[36] J.M. Freire, M.M. Domingues, J. Matos, M.N. Melo, A.S. Veiga, N.C. Santos, M.A. Castanho, Using zeta-potential measurements to quantify peptide partition to lipid membranes, Eur. Biophys. J. 40 (2011) 481–487.
[37] T. Yalçın, A. Alemdar, Ö.I. Ece, N. Güngör, The viscosity and zeta potential of bentonite dispersions in presence of anionic surfactants, Mater. Lett. 57 (2002) 420–424.
[38] K. Huus, S. Havelund, H.B. Olsen, M. van de Weert, S. Frokjaer, Thermal dissociation and unfolding of insulin, Biochemistry 44 (2005) 11171–11177.
[39] S. Benjwal, S. Verma, K.-H. Röhm, O. Gursky, Monitoring protein aggregation during thermal unfolding in circular dichroism experiments, Protein Sci. 15 (2006) 635–639.
[40] N. Poklar, J. Lah, M. Salobir, P. Maček, G. Vesnaver, pH and temperature-induced molten globule-like denatured states of equinatoxin II: a study by UV-melting, DSC, far- and near-UV CD spectroscopy and ANS fluorescence, Biochem. Mosc. 36 (1997) 14345–14352.
[41] A.M. Tsai, J.H. van Zanten, M.J. Betenbaugh, Study of protein aggregation due to heat denaturation: a structural approach using circular dichroism spectroscopy, nuclear magnetic resonance, and static light scattering, Biotechnol. Bioeng. 59 (1998) 273–280.
[42] A.W.P. Vermeer, W. Norde, The thermal stability of immunoglobulin: Unfolding and aggregation of a multi-domain protein, Biophys. J. 78 (2000) 394–404.
[43] L. Whitmore, B.A. Wallace, Protein secondary structure analyses from circular dichroism spectroscopy: Methods and reference databases, Biopolymers 89 (2008) 392–400.
[44] J.Y. Lim, N.A. Kim, D.G. Lim, K.H. Kim, S. Hada, S.H. Jeong, Evaluation of etanercept degradation under oxidative stress and potential protective effects of various amino acids, Int. J. Pharm. 492 (2015) 127–136.
[45] C.P.P. Pere, S.N. Economidou, G. Lall, C. Ziraud, J.S. Boateng, B.D. Alexander, D.A. Lamprou, D. Douroumis, 3D printed microneedles for insulin skin delivery, Int. J. Pharm. 544 (2018) 425–432.
[46] M.J. Ettinger, S.N. Timasheff, Optical activity of insulin. II. Effect of nonaqueous solvents, Bichemistry 10 (1971) 831–840.
[47] B. Sarmento, D. Ferreira, L. Jorgensen, M. Van De Weert, Probing insulin's secondary structure after entrapment into alginate/chitosan nanoparticles, Eur. J. Pharm. Biopharm. 65 (2007) 10–17.
[48] Z. Yong, D. Yingjie, W. Xueli, X. Jinghua, L. Zhengqiang, Conformational and bioactivity analysis of insulin: Freeze-drying TBA/water co-solvent system in the presence of surfactant and sugar, Int. J. Pharm. 371 (2009) 71–81.
[49] F. Andrade, P. Fonte, M. Oliva, M. Videira, D. Ferreira, B. Sarmento, Solid state formulations composed by amphiphilic polymers for delivery of proteins: characterization and stability, Int. J. Pharm. 486 (2015) 195–206.
[50] A.S. Ladokhin, M.E. Selsted, S.H. White, CD spectra of indolicidin antimicrobial peptides suggest turns, not polyproline helix, Biochemistry 38 (1999) 12313–12319.
[51] E. Terzi, G. Hoelzemann, J. Seelig, Reversible Random Coil-. Beta.-Sheet transition of the Alzheimer. Beta.-Amyloid Fragment (25-35), Biochemistry 33 (1994) 1345–1350.
[52] K.A. Conway, S.-J. Lee, J.-C. Rochet, T.T. Ding, R.E. Williamson, P.T. Lansbury, Acceleration of oligomerization, not fibrillization, is a shared property of both α-synuclein mutations linked to early-onset Parkinson's disease: implications for pathogenesis and therapy, Proc. Natl. Acad. Sci. USA. 97 (2000) 571–576.
[53] A.W. Vermeer, M.G. Bremer, W. Norde, Structural changes of IgG induced by heat treatment and by adsorption onto a hydrophobic Teflon surface studied by circular dichroism spectroscopy, Biochim. Biophys. Acta 1425 (1998) 1–12.
[54] T. Arakawa, K. Tsumoto, The effects of arginine on refolding of aggregated proteins:

not facilitate refolding, but suppress aggregation, Biochem. Biophys. Res. Commun. 304 (2003) 148–152.
[55] S. Ohtake, Y. Kita, T. Arakawa, Interactions of formulation excipients with proteins in solution and in the dried state, Adv. Drug Deliv. Rev. 63 (2011) 1053–1073.
[56] S.-L. Chiu, C.-M. Chen, H.T. Cline, Insulin receptor signaling regulates synapse number, dendritic plasticity, and circuit function in vivo, Neuron 58 (2008) 708–719.
[57] E. Steen, B.M. Terry, E.J. Rivera, J.L. Cannon, T.R. Neely, R. Tavares, J. Xu, J.R. Wands, S.M. de la Monte, Impaired insulin and insulin-like growth factor expression and signaling mechanisms in Alzheimer's disease–is this type 3 diabetes? J. Alzheimers Dis. 7 (2005) 63–80.
[58] K.I. Avgerinos, G. Kalaitzidis, A. Malli, D. Kalaitzoglou, P.G. Myserlis, V.-A. Lioutas, Intranasal insulin in Alzheimer's dementia or mild cognitive impairment: a systematic review, J. Neurol. (2018) 1–14.
[59] S. Alnajjar, H.K. Jin, J.E. Kang, S.H. Park, S.J. Rhie, Intranasal Insulin for Alzheimer's Disease and Amnestic Mild Cognitive Impairment: Systematic Review and Meta-analysis, Korean J. Clin. Pharm. 27 (2017) 161–170.
[60] R.R. Putheti, M.C. Patil, O. Obire, Nasal Drug delivery in Pharmaceutical and biotechnology: present and future, J. Sci. Technol. (2009) 4.
[61] H.R. Costantino, L. Illum, G. Brandt, P.H. Johnson, S.C. Quay, Intranasal delivery: physicochemical and therapeutic aspects, Int. J. Pharm. 337 (2007) 1–24.
[62] P. Arora, S. Sharma, S. Garg, Permeability issues in nasal drug delivery, Drug Discov. Today 7 (2002) 967–975.
[63] P.L. Privalov, S.A. Potekhin, Scanning microcalorimetry in studying temperature-induced changes in proteins, Methods Enzymol. 131 (1986) 4–51.
[64] C.H. Li, X. Nguyen, L. Narhi, L. Chemmalil, E. Towers, S. Muzammil, J. Gabrielson, Y. Jiang, Applications of circular dichroism (CD) for structural analysis of proteins: qualification of near- and far-UV CD for protein higher order structural analysis, J. Pharm. Sci. 100 (2011) 4642–4654.
[65] E. Marttin, N.G. Schipper, J.C. Verhoef, F.W. Merkus, Nasal mucociliary clearance as a factor in nasal drug delivery, Adv. Drug Deliver. Rev. 29 (1998) 13–38.
[66] C.P. Pujara, Z. Shao, M.R. Duncan, A.K. Mitra, Effects of formulation variables on nasal epithelial cell integrity: biochemical evaluations, Int. J. Pharm. 114 (1995) 197–203.
[67] C. Bitter, K. Suter-Zimmermann, C. Surber, Nasal drug delivery in humans, Curr. Probl. Dermatol. 40 (2011) 20–35.
[68] P.V. Jayakrishnapillai, S.V. Nair, K. Kamalasanan, Current trend in drug delivery considerations for subcutaneous insulin depots to treat diabetes, Colloid Surface B. 153 (2017) 123–131.